Int. J. Electrochem. Sci., 13 **(2018)** 10786 – 10797, doi: 10.20964/2018.11.21

International Journal of
ELECTROCHEMICAL
SCIENCE
www.electrochemsci.org

Electrochemical Behaviour of Tin in a LiCl-KCl Eutectic Melt

Yanqing Cai[1,*], *Xinggang Chen*[1], *Qian Xu*[2], *Ying Xu*[1]

[1] Hebei Provincial Key Laboratory of Inorganic Nonmetallic Materials, College of Material Science and Engineering, North China University of Science and Technology, Tangshan, China
[2] School of Materials Science and Engineering, Shanghai University, Shanghai, 200072, PR China
[*]E-mail: caiyanqing126@126.com

Received: 30 June 2018 / *Accepted:* 30 August 2018 / *Published:* 1 October 2018

The electrochemical behaviour and thermodynamic properties of $SnCl_2$ in a LiCl-KCl eutectic melt was investigated on graphite and Mo electrodes at 500°C by cyclic voltammetry, chronopotentiometry, square wave voltammetry, and open circuit chronopotentiometry. Two redox couples of tin ions due to Sn(IV)/Sn(II) and Sn(II)/Sn were obtained, and the cathodic peak potentials were found to be 0.50 V and -0.50 V, respectively. The reduction reactions of Sn(IV)/Sn(II) and Sn(II)/Sn are quasi-reversible processes and occur with two exchanged electrons, respectively. The diffusion coefficients of the Sn(IV) and Sn(II) ions were also determined on graphite electrode by the Berzins-Delahay equation, which were 2.68×10^{-5} cm^2/s and 5.19×10^{-5} cm^2/s, respectively. In addition, square wave voltammetry and open circuit chronopotentiometry experiments performed on a Mo electrode further indicated that the reduction of Sn(II) into Sn metal occurred in a single step and two electrons were exchanged. The research lays a foundation for electrolytic refining and electrodeposition of Zr−Sn alloy.

Keywords: molten chlorides, tin, diffusion coefficient, electrochemical behaviour

1. INTRODUCTION

Zirconium has a low absorption cross-section for thermal neutrons, high hardness and high corrosion resistance, which make it ideal for nuclear energy applications, such as cladding for fuel elements[1]. However, the strength and corrosion resistance of pure zirconium do not meet the requirements of nuclear industry applications[2, 3]. The preparation of zirconium-based alloys with improved overall performance is needed. Typical zirconium-based alloys include zirconium-tin and zirconium- niobium alloys[4]. Among these alloys, the zirconium-tin alloy (Zr−2 alloy) is composed of more than 95% zirconium and less than 2% tin, antimony, iron, chromium, and nickel, which are added to improve the mechanical properties and corrosion resistance of the alloy[5, 6]. Tin has important applications in electroplating, electronics, and synthetic alloys due to its low melting point and good

corrosion resistance, and one typical application is its use in zirconium-tin alloys[7].

Our research group plans to study the electrolytic refinement of zirconium-tin alloys and electrodeposition zirconium-tin alloys. The $ZrCl_4$ electrolyte is directly prepared by chlorinating Zr with $SnCl_2$, which has been reported in our previous work[8-10]. Due to the low potential of tin, it is expect to affect the purity of the $ZrCl_4$ electrolyte and the deposition of Zr in molten salt[11]. Therefore, it is highly important to study the electrochemical behaviour of tin ions in molten salt. There are many studies on the electrochemical behaviour of tin in aqueous solution [12-14]. However, since the aqueous solution contains hydrogen ions and zirconium is a metal with a deposition potential that is more negative than hydrogen, its refinement and preparation must be carried out in the molten salt[11, 15]. Thus, understanding the electrochemical behaviour of tin in molten salt is necessary.

Several investigators have studied the electrochemical behaviour of tin in molten chlorides. Ghallali[16, 17] investigated the electroreduction behaviours of Ni(II), Co(II) and Sn(II) for the synthesis of Ni–Sn and Co–Sn alloys and found that the reduction of Sn(II) ions occurs in a single two-electron step and that the process is diffusion controlled. The redox potential of Sn(II)/Sn is −1.39 V vs Cl_2/Cl^-, and the diffusion coefficient of Sn(II) ions was 2.7×10^{-5} cm^2 s^{-1} at 440 ◦C. Mikito[18] studied the electrochemical behaviours of Al(III) and Sn(II) ions for preparation of Al–Sn alloys for bearing materials. The results shows that the reduction of the Sn ions started at a potential of 0.5 V vs. Al/Al(III) in $AlCl_3$–NaCl–KCl–$SnCl_2$ molten salt at 423 K. Xu et.al[19] studied the electrochemical reduction of lithium and tin at graphite cathode in LiCl–KCl–4.5wt.%$SnCl_2$ at 625◦C. Two redox couples of Sn^{2+}/Sn and Sn^{4+}/Sn^{2+} were observed. The purpose was to investigate the difference in interaction of lithium in the metal/graphite electrode.

In summary, due to different research purposes and the complex electrochemical behaviour of Sn, which may consist of several stepwise processes, further studies are necessary. Thus, the present study focused on the redox step and cathodic deposition process of Sn in LiCl-KCl molten salt. The electrochemical behaviour and thermodynamic properties of $SnCl_2$ in LiCl-KCl eutectic melt were investigated on graphite and Mo electrodes at 500℃ by cyclic voltammetry, chronopotentiometry, square wave voltammetry, and open circuit chronopotentiometry. This work will provide basic research for the preparation of zirconium-tin alloys by electrolytic refinement and electrodeposition processes.

2. EXPERIMENTAL

All experiments were performed in a sealed homemade electric furnace, and the experimental procedure was maintained under an inert atmosphere of argon at 500 °C. A three-electrode electrochemical cell was assembled in an alumina crucible, which was placed in a stainless steel vessel and heated with the electric furnace[8]. The reference electrode (RE) was LiCl−KCl−1.0 wt.% AgCl molten salt placed in a close-ended mullite tube with a 1.0 mm (dia.) silver wire immersed in it for electrical connections. All potentials in this work will be referred to this electrode. The working electrodes were a spectrally pure graphite electrode (d = 6 mm) and a Mo electrode (d = 1 mm, 99.99%), respectively, and the counter electrode was a graphite electrode. All the electrodes were

extracted through the stainless steel wire. The experimental working electrode area was determined by measuring the immersion depth of the electrode in the salt after each experiment.

All the chemical reagents used in the experiment were analytically pure. The electrolyte was a LiCl−KCl (58.5:41.5 mol%) eutectic placed in an alumina crucible, dried for more than 72 h at 300 ℃ and later melted under an argon atmosphere. Moreover, to eliminate the residual water and other possible redox-active impurities, pre-electrolysis of LiCl−KCl melt was performed at 2.8 V for 2.0 h between two graphite electrodes prior to the electrochemical experiments. A certain amount of anhydrous $SnCl_2$ was added as the source of Sn(II). The anhydrous $SnCl_2$ was subjected to dehydration drying treatment before using. In the study of the electrochemical behaviour of Sn(II), an excess of 99.9% Sn particles was added to ensure the stability of Sn(II).

Electrochemical testing techniques such as cyclic voltammetry, chronopotentiometry, square wave voltammetry, and open circuit chronopotentiometry were tested by the AUTOLAB/PGSTAT320 potentiostat from M/s. EcoChemie, Netherlands controlled with GPES 4.9 software.

3. RESULTS AND DISCUSSION

3.1 Electrochemical behaviour of tin ions on graphite electrode

3.1.1 Cyclic voltammetry of tin ions in LiCl−KCl and LiCl−KCl−$SnCl_2$ on graphite electrode

To facilitate the electrochemical reaction mechanism of Sn(II), cyclic voltammograms (CVs) measurements were carried out in LiCl−KCl and LiCl−KCl−$SnCl_2$ melt on graphite electrodes at 773 K, as shown in Figure 1.

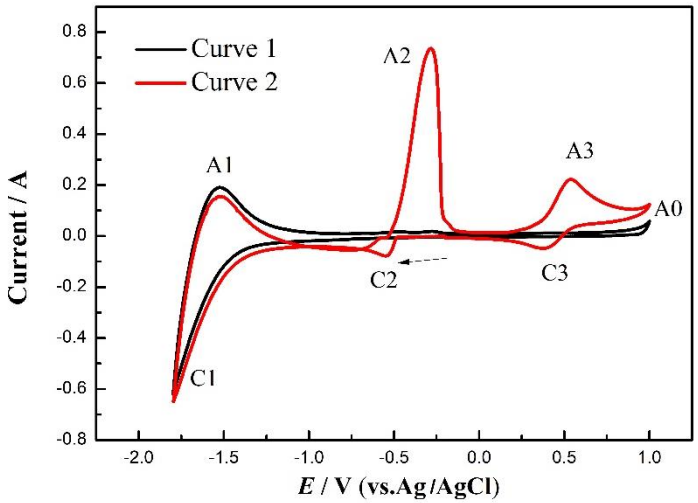

Figure 1. CVs for graphite electrode in (Curve 1) LiCl−KCl and (Curve 2) LiCl−KCl−$SnCl_2$ (0.13 wt.%) eutectic at 500 °C, S = 8.133 cm^2, scan rate: 0.05 $V \cdot s^{-1}$

Figure 1 shows a couple peaks of A1/C1 at a potential range from −1.25 to −1.75 V, which correspond to the deposition and dissolution of metal Li, respectively. The increase of the anodic current A0 is due to chlorine evolution[19]. Moreover, as seen in Curve 1, the residual current within a potential range from 1.00 to −1.00 V is less than 2 mA, and no current peaks are observed, which indicates that all reactions of impurities within this range are negligible.

Curve 2 shows the CV obtained after adding 0.13 wt.% $SnCl_2$ to LiCl−KCl molten salt. It can be seen that a cathodic peak C2 with a characteristic of metal deposition appears at −0.50 V, and a corresponding oxidation peak A2 appears at −0.30 V. Combined with the theoretical decomposition voltage of $SnCl_2$ in Equation (1), A2/C2 should represent the redox process of Sn(II)/Sn. Moreover, in the more positive potential region, a couple redox peaks of A3/C3 appear at approximately 0.50 V, corresponding to the redox couple of Sn(IV)/Sn(II) from Equation (2). The redox reaction of Sn ions is completed by a two-step two-electron exchange, which is the same as those reported by Xu [19] and Groult [20, 21], and the two resulting redox couples are Sn(IV)/Sn(II) and Sn(II)/Sn, respectively .

$$SnCl_2 = Sn + Cl_2(g) \qquad E^{\Theta}_{500℃}(\text{vs.Ag/AgCl}) = -0.214\text{V} \qquad (1)$$

$$SnCl_4(l) = SnCl_2 + Cl_2(g) \qquad E^{\Theta}_{500℃}(\text{vs.Ag/AgCl}) = 0.374\text{V} \qquad (2)$$

3.1.2 CVs of Sn(IV)/Sn(II) and Sn(II)/Sn at different scan rates

To further verify the number of exchanged electrons of Sn ions in the redox process, the CV for the graphite electrode under different scan rates was studied. Figure 2(a) shows a set of CVs obtained in LiCl−KCl−0.13wt.% $SnCl_2$ melt over a potential range of −0.90 to 0.90 V while changing scan rate from 0.05 to 1.0 V/s. Generally, it is believed that electrochemical reactions at lower scan rates fall within the category of reversible systems, and the number of exchanged electrons can be calculated over a low scan range. For reversible electrochemical reactions, the relationship between the potential difference (ΔE) of the oxidation peak and the reduction peak and the number of exchanged electrons are shown in Equation (3)[22, 23].

$$\Delta E = \left| E_{\text{pa}} - E_{\text{pc}} \right| = 2.3\text{R}T/n\text{F} \qquad (3)$$

where, n is the number of exchanged electrons, T is the absolute temperature, F is the Faraday constant, R is the standard gas constant, E_{pa} is the oxidation peak potential, and E_{pc} is the reduction peak potential.

Generally, the theoretical value ΔE for the reversible process of two exchanged electrons at 500 °C is 0.077 V[24]. For this experiment, when the scan rate is 0.05 V•s^{-1}, as shown in Table 1, the ΔE for the redox peaks A2/C2 and A3/C3 are 0.075 and 0.078 V, respectively, which are close to the theoretical values. This finding indicates that the A2/C2 and A3/C3 are the two-electron transfer redox processes, and are approximately reversible at low scan rate. As the scan rate increases, both the anode peak current and the cathode peak currents increase, and peak potentials move slightly. At a high scan rate (1.0 V•s^{-1}), ΔE for A2/C2 and A3/C3 are 0.130 and 0.237 V, respectively, which are considerably different from the theoretical value, indicating that the redox process cannot be regarded as a reversible process under a high scan rate. Moreover, as seen from the symmetry of redox peaks, the couple of A3/C3 has good symmetry, and that the anode peak current is equal to cathode peak current, which

explains why the reversibility of Sn(IV)/Sn(II) is better than that of Sn(II)/ Sn.

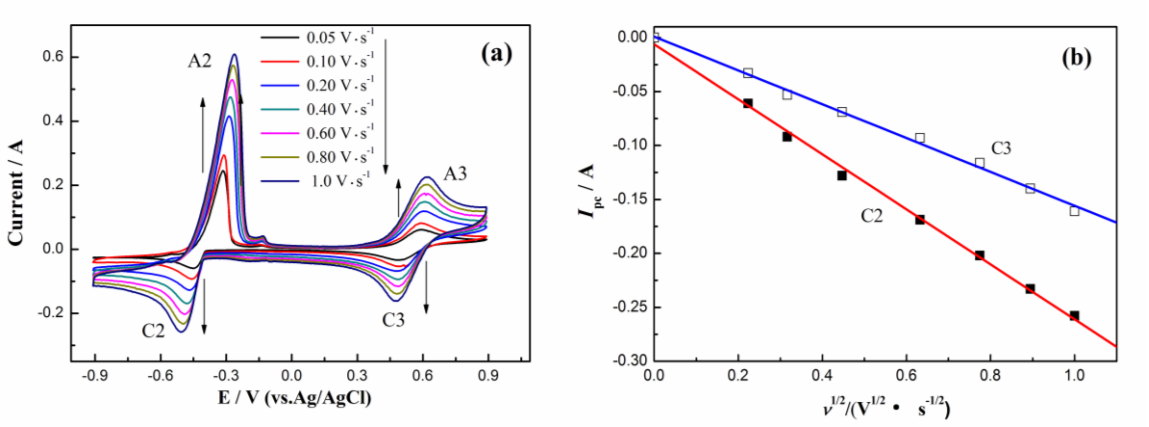

Figure 2. (a) CVs of LiCl−KCl−$SnCl_2$(1.01×10^{-5} mol·cm^{-3}) on a graphite electrode(S = 8.133 cm^2) at 500 °C with different scan rates (b) Variation of cathodic peak currents of C2 and C3 in (a) as a function of the square root of scan rates

Table 1. The potential difference at different scan rates

Scan rate	Δ*E* (A2/C2)	Δ*E* (A3/C3)
0.05 V·s^{-1}	0.075	0.078
1.0 V·s^{-1}	0.130	0.237

Figure 2(b) shows the linear relationship between the cathode peak currents of C2 and C3 and the square root of the scan rate. Moreover, the intercepts are the straight lines and the y-axis values are nearly zero, which is in accordance with the Berzins−Delahay equation, as shown in Equation (4)[24]. It can be inferred that the reduction processes of Sn(II) and Sn(IV) are controlled by the diffusion step. In addition, when the exchanged electron number n is two, the ion diffusion coefficients of Sn(IV) and Sn(II) can be obtained by Equation (4), which are 2.68×10^{-5} and 5.19×10^{-5} cm^2·s^{-1}, respectively. These ion coefficients are on the same order of magnitude as the diffusion coefficient found in the literature reported by Ghallali[16, 17], in which the diffusion coefficient of Sn(II) ions was 2.7×10^{-5} cm^2 s^{-1} at 440 ◦C.

$$I_p = 0.61(nF)^{3/2} A c_o D^{1/2} v^{1/2} (RT)^{-1/2} \qquad (4)$$

where I_p is the cathodic peak current (A), c_o is the bulk concentration of tin ions (mol·cm^{-3}), D is the diffusion coefficient (cm^2·s^{-1}), v is the potential scan rate (V·s^{-1}), A is the electrode surface area (cm^2), and the meanings of n, F, R, T are the same as those in Equation (3).

3.1.3 Chronopotentiometry on graphite electrode

To further confirm the reduction mechanism of Sn(II) and Sn(IV), chronopotentiometry was also performed in LiCl−KCl melt at different current densities on the graphite electrode, as shown in

Figure 3.

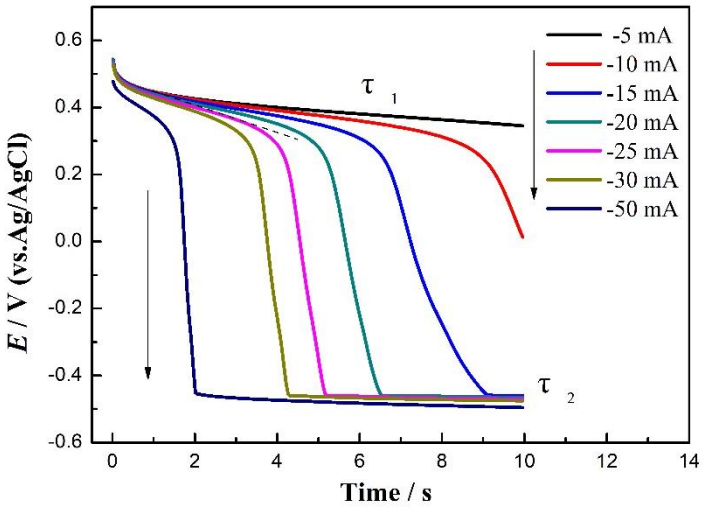

Figure 3. Chronopotentiograms obtained on the graphite electrode (S = 2.56 cm^2) in LiCl−KCl−$SnCl_2$(0.13 wt.%) at 500 °C with various cathodic currents

After applying a positive voltage of 0.6 V to the graphite electrode for 5 s, the chronopotentiometry on the graphite electrode was performed, and two distinct reduction steps were observed. Sn(II) was partially oxidized to Sn(IV) during the application of a positive voltage. Therefore, in the corresponding reduction process, two reduction platforms were present at 0.40 V and −0.50 V, corresponding to the reduction of Sn(IV) to Sn(II) and Sn(II) to Sn, respectively.

It is further demonstrated that Sn(II) is the intermediate valence state of Sn(IV) reduction, and the final reduction product is Sn metal. However, $SnCl_4$ is in a liquid state at normal temperature and is easily volatilized at the experimental operating temperature. For ease of operation, $SnCl_2$ is directly introduced into the melt for the chlorination process of zirconium as a reactive material.

3.2. Electrochemical behaviour of Sn(II)/Sn on Mo electrode

Since the redox potential of zirconium is more negative than that of tin, and the underpotential precipitation of Li occurs on the graphite electrode, the potential window of the graphite electrode cannot further satisfy the electrochemical behaviour investigation when tin and zirconium are present simultaneously. Therefore, a research electrode with a wide potential window between the deposition potentials of Sn(II) and Li(I) ions is needed. Thus, a Mo electrode, as a widely used, ideal inert electrode, is used as working electrode in the follow-up study.

3.2.1 Cyclic voltammetry of Sn(II)/Sn in LiCl−KCl and LiCl−KCl−$SnCl_2$ on Mo electrode

To further confirm the electrochemical behaviour of Sn(II) in LiCl–KCl melt, a series of CVs obtained at a Mo working electrode are shown in Figure 4. These measurements were carried out in

LiCl–KCl (curve 1) and LiCl–KCl−0.36 wt% $SnCl_2$ melt (curve 2), respectively. As shown in Curve 1, the cathodic peak A0 at −2.50 V vs. Ag/AgCl and the corresponding anodic peak A are observed, which correspond to the deposition and dissolution of Li. In Curve 2, the cathodic peak T' at −0.50 V corresponds to the reduction of Sn(II) to metallic Sn. Then, the corresponding anodic peak observed at −0.30 V is related to the oxidation of Sn to Sn(II)[20, 21]. Moreover, another three couples G_1/G_1' , G_2/G_2' and G_3/G_3' are obtained in the potential range from −2.0 to −2.5 V, which should correspond to the formation and dissolution of Sn–Li intermetallic compounds[19]. The results are consistent with the reported Sn–Li phase diagram[25], of four existing types of intermetallic compounds, i.e., Li_5Sn_2, $Li_{13}Sn_5$, Li_7Sn_2 and $Li_{22}Sn_5$. Among these compounds, the first two may be too close in composition to be distinguished by means of cyclic voltammetry, and the result is the same as those reported by Xu[19]. Moreover, the redox peak potential of Zr is at a potential range from −0.90 to −1.3 V, and the potential window of the Mo electrode can satisfy the electrochemical behaviour investigation when tin and zirconium are present simultaneously.

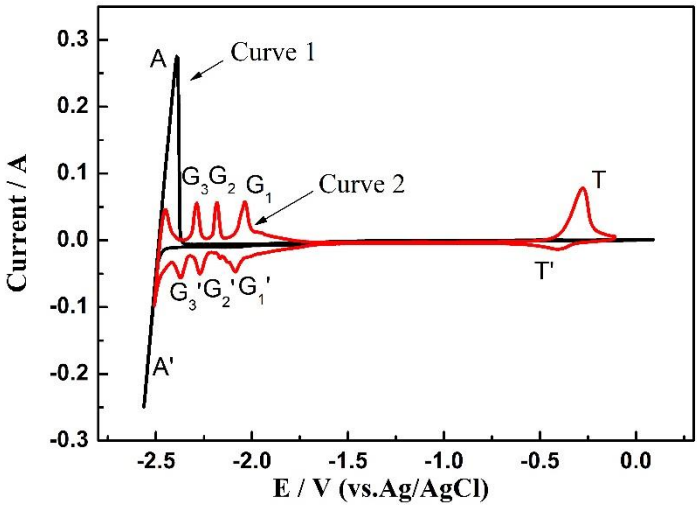

Figure 4. CVs of (Curve 1) LiCl−KCl melt, and (Curve 2) LiCl−KCl−$SnCl_2$ (0.36 wt.%) melt on Mo electrode at 500 °C. S= 0.628 cm^2, scan rate: 0.10 $V \cdot s^{-1}$

3.2.2 CVs of Sn(II)/Sn at different scan rates on Mo electrode

Figure 5(a) shows the CV of LiCl−KCl−$SnCl_2$ (0.36 wt.%) on Mo electrode at different scan rates. The scan range is 0～−0.6 V. As seen from Figure 5, the redox couple represents the deposition and oxidation processes of the Sn(II)/Sn, respectively. Consistent with the results obtained on the graphite electrode, the peak current gradually increased with the increase of the scan rate, and the peak potential gradually moved towards the scanning direction, indicating that the reversibility of the redox couple deteriorated at a high scan rate. Figure 5(b) shows a plot of cathode peak current as a function of scan rate, which is a linear relationship, indicating that the reduction process of Sn(II) ions is controlled by the diffusion step. For the Sn(II)/Sn soluble-insoluble system, the diffusion coefficient of Sn(II) ions can be calculated by the Berzins−Delahay equation[24], as shown in Equation (4), and the

final calculation result is 1.54×10^{-5} $cm^2 \bullet s^{-1}$. This is on the same order of magnitude as the result obtained by cyclic voltammetry on graphite electrodes, and agrees with the results calculated by Ghallali[16, 17].

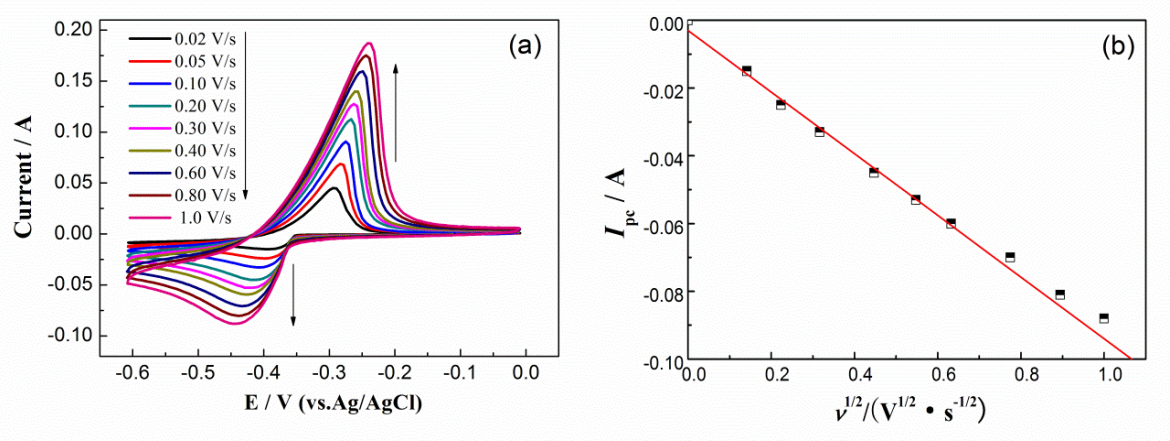

Figure 5. (a) CVs of LiCl−KCl−$SnCl_2$ (0.36 wt.%) on Mo electrode (S =0.628 cm^2) at 500 °C with different scan rates, (b) Variation of cathodic peak currents as a function of scan rates

3.2.3 Square wave voltammetry of Sn(II)/Sn on Mo electrode

Square wave voltammetry was also performed to further monitor the redox process of the Sn(II)/Sn couple[26, 27]. Figure 6 shows a group of square wave voltammograms (SWVs) observed at different frequencies in LiCl−KCl−$SnCl_2$ (0.36 wt.%) molten salt. There is an incompletely symmetric peak at −0.33 V at a frequency of 25 Hz and a step potential of 1 mV. The asymmetry may be caused by the overpotential generated by the reduction of Sn(II) ion to the liquid Sn metal, which is consistent with the phenomenon of liquid metal deposition in the literature [28].

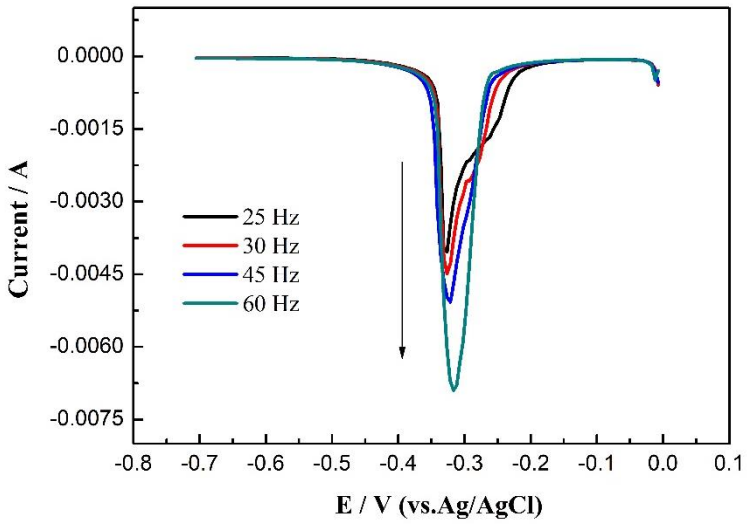

Figure 6. SWVs of LiCl−KCl−$SnCl_2$(0.36 wt.%) on Mo electrode (S =0.628 cm^2) at 500 °C with different frequencys. Potential step: 1 mV, pulse height: 15 mV

In addition, the peak potential changes only slightly with the increase of frequency, which indicates that the reduction of Sn(II) is a quasi-reversible system, and the exchanged electron number of the reduction reaction can be approximated by Equation (5). When calculating the number of exchanged electrons, the interference based on the nucleation effect must be eliminated in consideration of the effect of the half-peak width. When the frequency is 25 Hz, the half width of the reduction peak is 0.04 V, and the exchanged number is calculated to be 1.66, which is approximately equal to 2. This indicates that the reduction of Sn(II) to metal Sn is a one step and two electron transfer process. This is consistent with the two-electron reduction reaction of Sn(II) to Sn in Equation (1) presumed by cyclic voltammetry.

$$W_{1/2} = 3.52RT / nF \qquad (5)$$

where $W_{1/2}$ is half-peak width, the meanings of n, F, R, T are the same as those in Equation (3).

3.2.4 Chronopotentiometry of Sn(II)/Sn on Mo electrode

Chronopotentiometry was also performed to observe the redox process of the Sn(II)/Sn couple. Figure 7(a) shows the chronopotentiometry of the Mo electrode at different current intensities in LiCl−KCl−$SnCl_2$ (0.36 wt.%) molten salt.

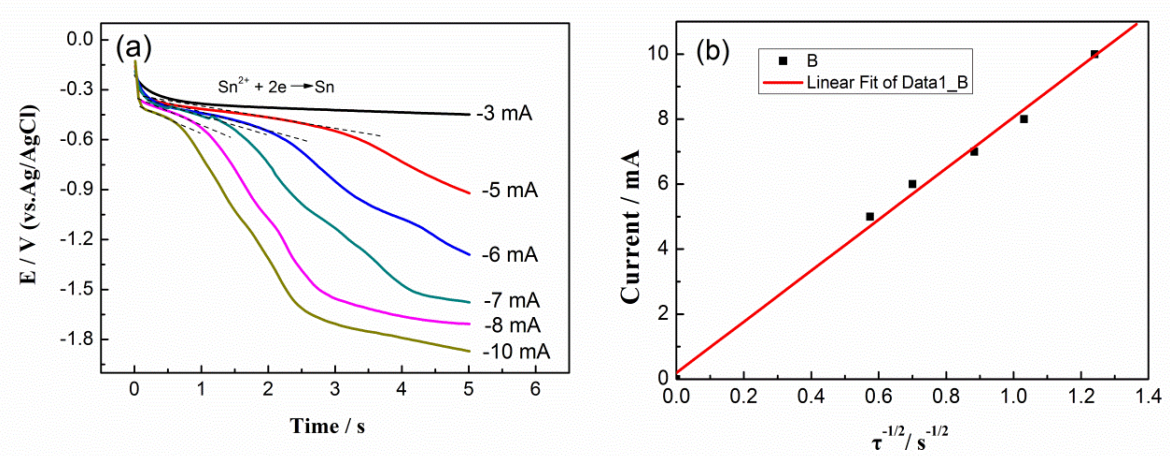

Figure 7. (a) Chronopotentiograms obtained at different current intensities for LiCl−KCl−$SnCl_2$ (0.36 wt.%) eutectic at 500 °C, and (b) the relationship between i and $\tau^{-1/2}$, S = 0.628 cm^2

As seen from Figure 7(a), a potential platform appears at around −0.40 V, corresponding to the reduction process of Sn(II) to Sn. As the current intensity increases, the negative shift of the potential platform is not obvious, indicating that the reduction process of Sn(II) is subjected to the diffusion control process. In addition, as the current intensity increases continuously, a new potential platform begins to appear at −1.70 V, which may be caused by the decomposition of undecomposed moisture, or an intermetallic compound formation process of Li−Sn[20]. Figure 7(b) shows the relationship between the different current intensities and the reciprocal of the square root of the transition time, which is a linear relationship. Therefore, the Sand equation [24] can be used to calculate the diffusion coefficient of Sn(II) from the slope of the straight line, as shown in Equation (6). Finally, the diffusion coefficient of Sn(II) is calculated to be 1.69×10^{-5} $cm^2 \cdot s^{-1}$, which is on the same order of magnitude as

the diffusion coefficient obtained by cyclic voltammetry and that also found in the work by Ghallali[16, 17].

$$I = 0.5nFAD^{1/2}\pi^{1/2}c_0\tau^{-1/2} \quad (6)$$

where I is the current intensity (A), τ is the transition time, and the meanings of n, F, R, T, A, D, c_o are the same as those in Equation (4).

3.2.5 Open−circuit chronopotentiometry of Sn(II)/Sn on Mo electrode

To further understand the deposition and dissolution process of tin on Mo electrode, the open−circuit chronopotentiometry on Mo electrode in LiCl−KCl−$SnCl_2$ molten salt was studied. First, a negative potential (−2.60 V) was applied for 10 seconds to the Ag/AgCl electrode on the Mo electrode. Next, the power was turned off, and the curve of the electrode potential with time was recorded. Figure 8 illustrates the open circuit chronopotentiogram (OCP) of the Mo electrode in LiCl−KCl−$SnCl_2$ (0.36 wt.%) molten salt.

As seen in Figure 8, the open circuit potential slowly shifts positively with time, and several potential platforms appear. First, a potential platform *a* appears at around −2.50 V, which corresponds to the dissolution of the deposited Li metal. Subsequently, potential platforms b_1, b_2, and b_3 appear at −2.33, −2.22, and −2.07 V, respectively, which correspond to the several intermetallic compounds formed by Sn and Li. Finally, the potential platform *c* generates at −0.38 V, which represents the deposition and dissolution of the Sn metal. The chronopotentiometry results are in good agreement with the cyclic voltammetry results obtained in section 3.2.1, which also illustrates the redox behaviour of Sn(II)/Sn in LiCl−KCl−$SnCl_2$ molten salt.

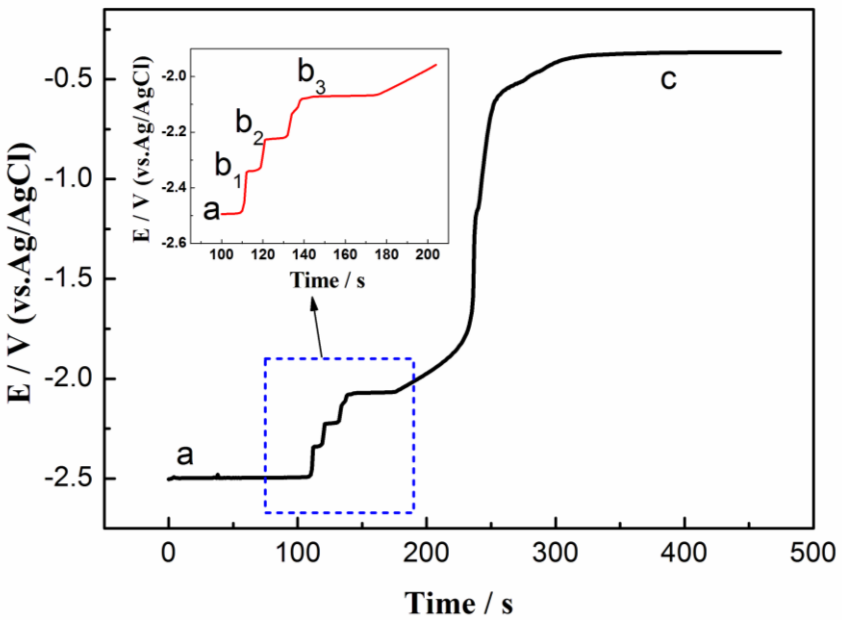

Figure 8. OCP of LiCl−KCl− $SnCl_2$ (0.36 wt.%) melt after electrodepositing at −2.60 V vs. Ag/AgCl for 10 s on Mo electrode (S=0.628 cm^2) at 500 °C

4. CONCLUSION

The electrochemical behaviour of Sn in LiCl−KCl−$SnCl_2$ and thermodynamic properties were studied on graphite and Mo electrodes at 500℃ with a series electrochemical techniques, including cyclic voltammetry, square wave voltammetry, chronopotentiometry, and open−circuit chronopotentiometry. Two reduction potentials of tin ions were obtained at 0.50 V and −0.50 V on a graphite electrode, which correspond to Sn(IV)/Sn(II), Sn(II)/Sn couples, respectively. The results showed that the reduction of Sn(IV)/Sn(II) and Sn(II)/Sn are quasi−reversible processes controlled by diffusion mass transfer. The diffusion coefficients of Sn(IV) and Sn(II) were calculated by the results of cyclic voltammetry on the graphite electrode, which are 2.68×10^{-5} and 5.19×10^{-5} $cm^2 \cdot s^{-1}$, respectively. Meanwhile, the electrochemical behaviour of Sn(II)/Sn couple was also investigated in detail on the Mo electrode, and the results of square wave voltammetry and open-circuit chronopotentiometry further indicate that the reduction of Sn(II) ions into Sn metal occurs in a single step with two exchanged electrons. The study of this study lay a foundation for future research in electrorefining and electrodeposition of Zr−Sn alloy.

ACKNOWLEDGEMENTS
The authors acknowledge the National Science Foundation of China (Grant No. 51804124), Hebei Natural Science Foundation of China (Grant No. E2017209128), Applied Basic Research Project of Tangshan City (Grant No.18130238a), and Doctoral Research Start−up Project of North China University of Science and Technology (Grant No.28407399).

References

1. M. Gibilaro, L. Massot, P. Chamelot, L. Cassayre, P. Taxil. *Electrochim. Acta*, 95(2013)185.
2. Z. Chen, Y.J. Li, S.J. Li. *J. Alloys Compd.*, 509(2011)5958.
3. C. Guang-Sen, M. Okido, T. Oki. *J. Appl. Electrochem.*, 20(1990)77.
4. C.H. Lee, K.H. Kang, M.K. Jeon, C.M. Heo, Y.L. Lee. *J. Electrochem. Soc.*, 159(2012)D463.
5. M. Große, E. Lehmann, M. Steinbrück, G. Kühne, J. Stuckert. *J. Nucl. Mater.*, 385(2009)339.
6. W.Q. Liu, Q. Li, B.X. Zhou, Q.S. Yan, M.Y. Yao. *Rare Metal Mat. Eng.*, 26(2007)104.
7. Y.H. Jeong, J.H. Baek, B.K. Choi, M.H. Lee, S.Y. Park, C. Nam, Y.H. Jung. US; 2004.
8. Y.Q. Cai, H.X. Liu, Q. Xu, Q.S. Song, H.J. Liu. *Int. J. Electrochem. Sci.*, 10(2015)4324.
9. Y.Q. Cai, H.X. Liu, Q. Xu, Q.S. Song, H.J. Liu. *RSC Adv.*, 5(2015)31648.
10. Y.Q. Cai, H.X. Liu, Q. Xu, Q.S. Song, L. Xu. *Electrochim. Acta*, 161(2015)177.
11. P.J. Sohn Sungjune, Hwang Il Soon. *Int. J. Electrochem. Sci.*, 13(2018)3897.
12. L.D.L. Tang J, Xu C Y. *Int. J. Electrochem.*, 2018(2018)1.
13. T. Nan, J. Yang, B. Chen. *Ultrason. Sonoche.*, 42(2018)731.
14. N.F.E. Boraei, S.S.A.E. Rehim. *Mater. Chem. Phys.*, 215(2018)332.
15. D. Quaranta, L. Massot, M. Gibilaro, E. Mendes, J. Serp, P. Chamelot. *Electrochim. Acta*, 265(2018)586.
16. H. El Ghallali, H. Groult, A. Barhoun, K. Draoui, D. Krulic, F. Lantelme. *Electrochim. Acta*, 54(2009)3152.
17. H. Groult, H. El Ghallali, A. Barhoun, E. Briot, L. Perrigaud, S. Hernandorena, F. Lantelme. *Electrochim. Acta*, 55(2010)1926.
18. M. Ueda, R. Inaba, T. Ohtsuka. *Electrochim. Acta*, 100(2013)281.

19. Q. Xu, C. Schwandt, D.J. Fray. *J. Electroanal. Chem.*, 562(2004)15.
20. H. Groult, H.E. Ghallali, A. Barhoun, E. Briot, C.M. Julien, F. Lantelme, S. Borensztjan. *Electrochim. Acta*, 56(2011)2656.
21. H.E. Ghallali, H. Groult, A. Barhoun, K. Draoui, D. Krulic, F. Lantelme. *Electrochim. Acta*, 54(2009)3152.
22. N. Tachikawa, N. Serizawa, Y. Katayama, T. Miura. *Electrochim. Acta*, 53(2008)6530.
23. M. Li, X.L. Xi, Z.R. Nie, L.W. Ma, Q.Q. Liu. *Int. J. Electrochem. Sci.*, 13(2018)4208.
24. A.J. Bard, L.R. Faulkner. Electrochemical methods: fundamentals and applications: Wiley& Sons Inc, (1981) New York, America.
25. W.G. Moffatt. The handbook of binary phase diagrams: Genium Pub. Corp.; 1976.
26. K. Liu, Y.L. Liu, L.Y. Yuan, X.L. Zhao, Z.F. Chai, W.Q. Shi. *Electrochim. Acta*, 109(2013)732.
27. H. Tang, Y.D. Yan, M.L. Zhang, X. Li, Y. Huang, Y.L. Xu, Y. Xue, W. Han, Z.J. Zhang. *Electrochim. Acta*, 88(2013)457.
28. Y.L. Liu, Y.D. Yan, W. Han, M.L. Zhang, L.Y. Yuan, R.S. Lin, G.A. Ye, H. He, Z.F. Chai, W.Q. Shi. *Electrochim. Acta*, 114(2013)180.